Hindawi
Mathematical Problems in Engineering
Volume 2019, Article ID 8729125, 12 pages
https://doi.org/10.1155/2019/8729125

Research Article

Vector Weighting Approach and Vector Space Decoupling Transform in a Novel SVPWM Algorithm for Six-Phase Voltage Source Inverter

Peng Wu,[1] Lei Yuan ,[2] Zhen Zuo,[1] and Junyu Wei[3]

[1]*College of Artificial Intelligence, National University of Defense Technology, Changsha, 410073, China*
[2]*Institute of Communications Engineering, The Army Engineering University of PLA, Nanjing, 210007, China*
[3]*College of Electric and Information Engineering, Hunan University of Technology, Zhuzhou 412007, China*

Correspondence should be addressed to Lei Yuan; lei.yuan.v@qq.com

Received 12 February 2019; Revised 13 April 2019; Accepted 6 May 2019; Published 13 June 2019

Academic Editor: Zhixiang Zou

For six-phase permanent-magnet synchronous motor (PMSM) which has two sets of Y-connected three-phase windings spatially phase shifted by 30 electrical degrees, to increase the utilization ratio of the DC bus voltage, a novel space vector pulse width modulation (SVPWM) algorithm in full modulation range capability based on vector weighted method is proposed in this paper. The basic vector action time of SVPWM method is derived in detail, employing vector space decomposition transformation approach. Compared with the previous algorithm, this strategy is able to overcome the inherent shortcomings of the four-vector SVPWM, and it achieves smooth transitions from linear to overmodulation region. Simulation and experimental analyses demonstrate the effectiveness and feasibility of the proposed strategy.

1. Introduction

Compared with the pulse width modulation (PWM) control algorithm for conventional three-phase motors, the PWM method for six-phase motors is more flexible [1–6]. At present, carrier-type PWM algorithm, permanent-magnet synchronous motor SVPWM algorithm, and current hysteresis PWM algorithm are three of the PWM algorithms that are commonly used for multiphase two-level voltage source inverter (VSI) [7, 8]. However, the current hysteresis PWM algorithm is unsuitable for high power algorithms. In recent years, carrier-type PWM algorithms and SVPWM algorithms that can be applied to multiphase motor systems have been extensively studied.

The PWM algorithm for multiphase inverters aims to eliminate low-order harmonic components as much as possible, which is different from that for the three-phase motor system [9–11]. As these low-order harmonic components could result in the loss of the motor by leading to a large amount of stator harmonic current components in the x-y subspace. In order to increase the utilization ratio of the DC bus voltage, multiphase carrier-type PWM algorithm based on zero-sequence signal injection is applied for multiphase inverter system which is composed of several three-phase windings. In particular, the reference voltage vector can be decomposed into two three-phase inverters sharing a common DC bus voltage when used in practice. After that, the carrier-type PWM algorithm based on dual zero-sequence injection can be used [12, 13]. Although this method is easy for digital realization, it is not an optimal PWM algorithm for multiphase motors as there are fifth and seventh harmonic components in the stator current.

As the multiphase AC motors have been widely used, the conventional inverter control algorithm is expected to be optimized for them. At present, many researches are devoted to the implementation of the SVPWM algorithm. One of the multiphase SVPWM algorithms is based on the maximum adjacent two vectors, in which the voltage of the subspace is sinus without considering the influence of the x-y subspace voltage [14]. In this connection, there are more harmonic voltages in the output and a larger fundamental voltage modulation factor can be gotten in this way [15]. While for

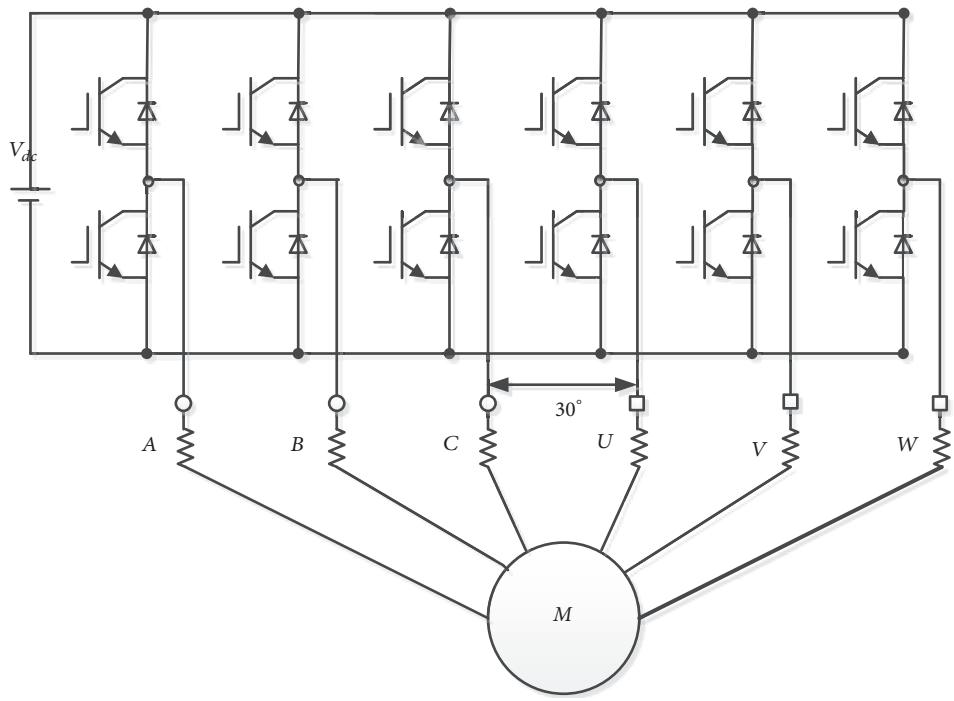

Figure 1: Six-phase converter drive system.

multiphase AC motors, the SVPWM algorithm will become incredibly complex. And with the increase of the number of motor phases, the complexity of this direct calculation SVPWM algorithm will be greatly increased: sector judgment, vector duration calculation, vector action sequence arrangement, vector duration conversion into switching action time, and other complex issues and the difficulty will be greatly increased, and the performance requirements of the controller will undoubtedly be greatly improved.

In order to further improve the DC bus utilization rate, a two-vector and improved four-vector algorithm can be used to increase the modulation factor by injecting the 5th and 7th harmonics of the vector in the x-y subspace. This method only increases the system loss and does not generate torque ripple. But it only reached the maximum linear modulation range. When it is necessary to continue to improve the bus voltage utilization rate, it can be said that the commonly used three-phase overmodulation technology [16, 17] is extended to the six-phase system, and the 11th and 13th harmonics are injected in the α-β subspace, so that the maximum bus voltage utilization can be obtained. However, the torque ripple will be poor.

In order to increase the utilization ratio of the DC bus voltage, numerous studies have been done on improving the PWM algorithm for three-phase motor when overmodulation occurs. As for the PWM overmodulation strategies for multiphase motors, the fundamental amplitude of the output reference voltage will rise by using vector space decomposition (VSD) in [10] transform matrix decomposition to get fundamental component of the x-y subspace [18] while the harmonic content of the reference voltage in the linear modulation region also increases in that way.

To solve above problems, and to increase the utilization ratio of the DC bus voltage, a novel SVPWM algorithm for six-phase VSI with wide modulation range capability based on vector weighted method is proposed in this paper. The concept of mid-vector presented in [18] is employed to obtain the expression for the time of algorithm of the active space voltage vectors, and using vector weighted method, the overmodulation region is divided into three sections, and the proposed SVPWM algorithm can also allow smooth transition from a linear modulation region to an overmodulation region. The control strategy is verified through simulation analysis.

2. Dwell Time Calculation for Six-Phase VSI

The six-phase motor system fed by six-phase VSI is shown in Figure 1. There are two sets of Y-coupled three-phase stator windings, which are spatially separated by 30° electrical degrees. Since there are two switch states for each bridge arm, the six-phase inverter has 2^6 switch states. According to the VSD transformation approach, all of the space vectors can be mapped to the α-β, x-y, and o1-o2 three mutually orthogonal subspaces. The fundamental component and harmonics with the order 12n±1 (n=1, 2, 3,...) are mapped into the α-β subspace. The harmonics with the order 6n±1 (n=1, 3, 5,...) and the harmonics with the order 6n±3 (n=1, 3, 5,...) are mapped into the x-y subspace and the o1-o2 subspace, respectively. The subspaces are divided into 12 sectors.

To suppress the harmonic current component of stator current, a good four-vector SVPWM method should satisfy that the amplitude of the reference voltage vector in the α-β subspace is maximum, and in the x-y subspace is minimum.

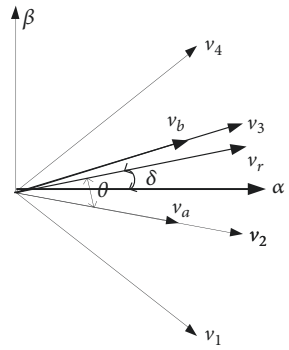

Figure 2: SVPWM method based mid-vector.

In the α-β subspace, any three adjacent voltage vectors can be synthesized into a new vector, called mid-vector, and the mid-vector has a same direction as the vector in the middle position. As shown in Figure 2, three adjacent basic vectors v_1, v_2, and v_3 are employed to synthesize into a mid-vector v_a. Supposing the dwell time of vector v_2 is aT_s, the vectors v_1 and v_3 will be 0.5(1-a) T_s. The amplitude of v_a in α-β subspace and x-y subspace, respectively, are as follows:

$$\left|v_{\max}{}'\right| = \frac{\sqrt{2}\left(\sqrt{3}+1\right)}{6} V_{dc}\left(a + \frac{\sqrt{3}}{2}(1-a)\right) \quad (1)$$

$$\left|v_{\min}{}'\right| = \frac{\sqrt{2}\left(\sqrt{3}-1\right)}{6} V_{dc}\left(a - \frac{\sqrt{3}}{2}(1-a)\right) \quad (2)$$

where a is a positive constant.

Similarly, the three adjacent basic vectors v_2, v_3, and v_4 are employed to synthesize into a mid-vector v_b. In this way, we can synthesize 12 voltage vectors which have the same distribution as the traditional two vector SVPWM algorithm, but the magnitude is different. So the reference voltage vector v_r in α-β subspace can be synthesized by using 12 mid-vectors, and the basic principle is the same as the traditional two vector SVPWM algorithm, the dwell time of mid-vectors Ta and Tb can be calculated according to (5), and $|v_{\max}|$ must be replaced by the variable $|v_{\max}{}'|$, and the dwell time of vectors v_1, v_2, v_3, and v_4 can be obtained by

$$\begin{aligned} t_1 &= 0.5(1-a)T_a \\ t_2 &= aT_a + 0.5(1-a)T_b \\ t_3 &= 0.5(1-a)T_a + aT_b \\ t_4 &= 0.5(1-a)T_b \end{aligned} \quad (3)$$

Moreover, the relationship between θ and δ is obtained by

$$\theta = \delta + \frac{\pi}{12} - \frac{k-1}{6}\pi \quad (4)$$

where k is the sector, with k=1,2, 3. . .12.

According to the traditional three-phase SVPWM method, the dwell time of mid-vector can be used by

$$T_a = \frac{|v_r|}{|v_{\max}|\sin(\pi/6)} \sin\left(\frac{2k-1}{12}\pi - \delta\right) T_s$$

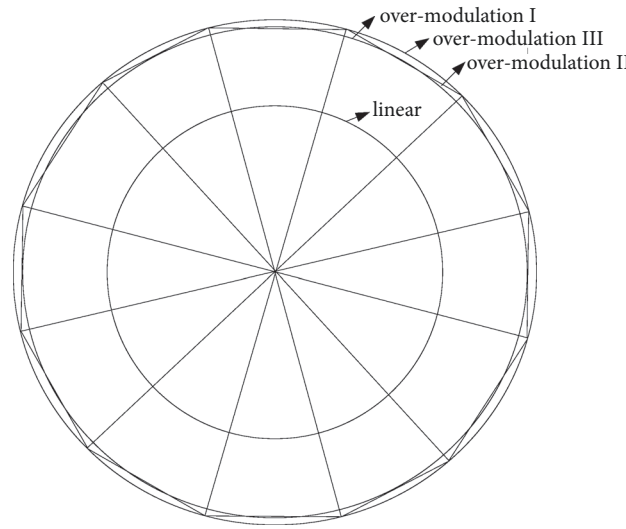

Figure 3: Linear and overmodulation range.

$$T_b = \frac{|v_r|}{|v_{\max}|\sin(\pi/6)} \sin\left(\delta - \frac{2k-3}{12}\pi\right) T_s \quad (5)$$

where Ts is the switch period and $|v_r|$ is the amplitude of the reference voltage vector.

In the linear modulation range, the control objective of four-vector SVPWM based on mid-vector method is to reduce the current harmonic component; i.e., the amplitude of reference is maximum in the α-β subspace and minimum in the x-y subspace. For this purpose, (1) is only to be satisfied with $|v_{\min}{}'| = 0$, i.e., $a = 2\sqrt{3} - 3$. Equation (2) will change into $|v_{\max}{}'| = (3\sqrt{2} - \sqrt{6})/3 \cdot V_{dc}$. The dwell time of mid-vector can be obtained by replacing $|v_{\max}|$ with $|v_{\max}{}'|$, and then the expression of dwell time can be achieved by (3).

3. A Novel SVPWM Technology with Wide Modulation Range

3.1. Overmodulation Region Division. To facilitate the analysis, the modulating index is defined by

$$m = \frac{\pi |v_r|}{(2V_{dc})} \quad (6)$$

when the reference voltage vector is more than this limiting value of $|v_r| = 2V_{dc}/\sqrt{3}$ and the inverter moves into the overmodulation region for $2V_{dc}/\sqrt{3} < |v_r| < 2V_{dc}/\pi$. When the voltage vector is $|v_r| = 2V_{dc}/\pi$, the inverter operates in the twelve-step mode, as shown in Figure 3.

The overmodulation region is further divided into three submodes, the overmodulation region I ($0.907 < m \leq 0.977$), the overmodulation region II ($0.977 < m \leq 0.988$), and the overmodulation region III ($0.988 < m \leq 1$).

3.2. SVPWM Based on Vector Weighted Method. When the system is running in different overmodulation region as

shown in Figure 3, the basic idea of vector weighting method is to obtain a new integrated reference voltage vector by weighting the voltage vectors in different overmodulation regions, with using the concept of modulation coefficient, and use the reference voltage vector to calculate the duty cycle of PWM. In order to facilitate calculation, four voltage vectors are defined in this paper, such as $V_{\sin1}$, $V_{\sin2}$, V_{dod}, and V_{twe}. $V_{\sin1}$ is the voltage vector of the maximum linear modulation ratio when the four vector SVPWM algorithm is used, and the trajectory is a circle with a radius of $V_{dc}/\sqrt{3}$. $V_{\sin2}$ is the voltage vector corresponding to the two-vector SVPWM algorithm, and the trajectory is a dodecagon inscribed circle with a radius of $\sqrt{2}(\sqrt{3}+1)/6 \cdot V_{dc} \cdot \cos(\pi/12)$. V_{dod} is the voltage vector that rotates on the contour line of regular dodecagon. V_{twe} is the voltage vector of twelve-step wave. The expression of the four voltage vectors will be shown as follows:

$$V_{\sin1} = \frac{V_{dc}}{\sqrt{3}} e^{j\delta} \approx 0.577 V_{dc} \cdot e^{j\delta} \tag{7}$$

$$V_{\sin2} = \frac{\sqrt{2}\left(\sqrt{3}+1\right)V_{dc}}{6} \cos\frac{\pi}{12} e^{j\delta} \approx 0.622 V_{dc} \cdot e^{j\delta} \tag{8}$$

$$\begin{aligned} V_{dod} &= \frac{\sqrt{2}\left(\sqrt{3}+1\right)V_{dc}}{6\cos\left(\left(\left(2\left(k-1\right)+1\right)/12\right)\pi-\theta\right)} \cos\frac{\pi}{12} e^{j\delta} \\ &\approx \frac{0.622 V_{dc}}{\cos\left(\left(\left(2\left(k-1\right)+1\right)/12\right)\pi-\theta\right)} e^{j\delta} \end{aligned} \tag{9}$$

$$\begin{aligned} V_{twe} &= \frac{\sqrt{2}\left(\sqrt{3}+1\right)V_{dc}}{6} e^{jk(\pi/12)} \\ &\approx 0.644 V_{dc} \cdot e^{jk(\pi/12)}, \quad \frac{k-1}{6}\pi \le \delta \le \frac{k}{6}\pi \end{aligned} \tag{10}$$

where δ is the angle between reference voltage vector v_r and α axis, the relationship between $V_{\sin1}$, $V_{\sin2}$, V_{dod}, and v_r is phase equality, and the amplitude of four-vector is $0.577V_{dc}$, $0.622V_{dc}$, $0.629V_{dc}$, and $0.6366V_{dc}$.

3.2.1. Overmodulation Region I ($0.907 < m \le 0.977$). It can be seen from (1) and (2) that the amplitude $|v_{\max}{}'|$ of fundamental voltage vector will gradually become larger with an increase of a, but the amplitude of harmonic subspace voltage vector will also gradually increase. The modulation method especially will become two-vector SVPWM algorithm. To obtain the reference voltage vector v_r, the amplitude need to be satisfied with $|v_r| = |v_{\max}{}'|\cos(\pi/12)$; it can be obtained as follows:

$$a = 12\frac{|v^*|}{V_{dc}} - 2\sqrt{3} - 3 \tag{11}$$

The unitary expression of dwell time can be achieved when (11) is substituted into (1), with considering function (3). When the reference voltage vector v_r is in the modulation region I, the amplitude of v_r will gradually increase to $0.622V_{dc}$, and the value of a will also gradually increase from $2\sqrt{3}-3$ to 1. Thus, the smooth transition from linear modulation region to overmodulation region I is realized.

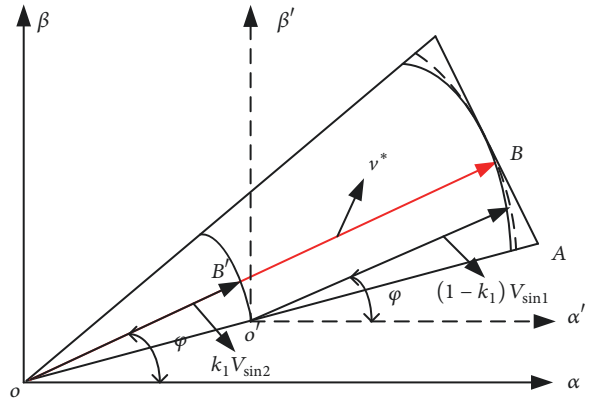

Figure 4: The principle diagram reference voltage vector in overmodulation section.

According to the principle of vector weighting method, the overmodulation coefficient of overmodulation I is defined as

$$k_1 = \frac{m - m_1}{m_2 - m_1}, \quad (0 \le k_1 \le 1) \tag{12}$$

where m_1=0.907 and m_2=0.977. The value k_1 will be set to 0 when the vector v_r is in linear modulation region, and the value k_1 is set to 1 when v_r rotates along the inner-circle of the regular dodecagon.

Like overmodulation I region, to illustrate the process of adjusting the reference voltage vector, sector 2 shown in Figure 4 will be taken as an example, and $V_{\sin1}$ and $V_{\sin2}$ will be used to reconstruct the reference voltage vector v^*, i.e.,

$$v^* = \left(1-k_1\right)V_{\sin1} + k_1 V_{\sin2} \tag{13}$$

According to (7) and (8), the expression of v^* in sector 2 can be obtained by

$$\begin{aligned} |v^*| &= \frac{V_{dc}}{\sqrt{3}}\left(1-k_1\right) \\ &+ \frac{2\left(\sqrt{3}+1\right)^2 V_{dc}}{24}\left(a + \frac{\sqrt{3}}{2}\left(1-a\right)\right) \cdot k_1 \end{aligned} \tag{14}$$

The function (14) is substituted into (5), with considering (3), so the dell time of nonzero vector of each sector can be calculated and then get the PWM waveform of the overmodulation I.

Figure 5 shows the A phase voltage curve, in which V_{dc}=1V, and modulation ratio m increased from 0.907 to 0.977. As can be seen from the figure, with the gradual increase of modulation ratio m, the output voltage of the A phase voltage has a certain distortion. When m is close to 0.977, the reference voltage vector rotates along the inner-circle of the regular dodecagon.

3.2.2. Overmodulation Region II ($0.977 < m \le 0.988$). When the vector v_r is in overmodulation II, the outside of the regular dodecagon cannot be synthesized by the switch

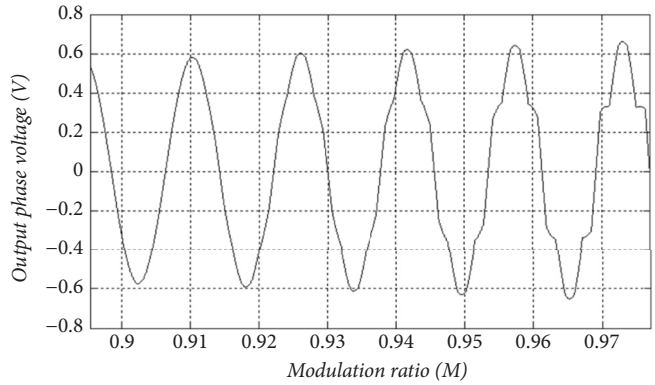

Figure 5: The relationship between fundamental amplitude of output phase voltage and m in mode I.

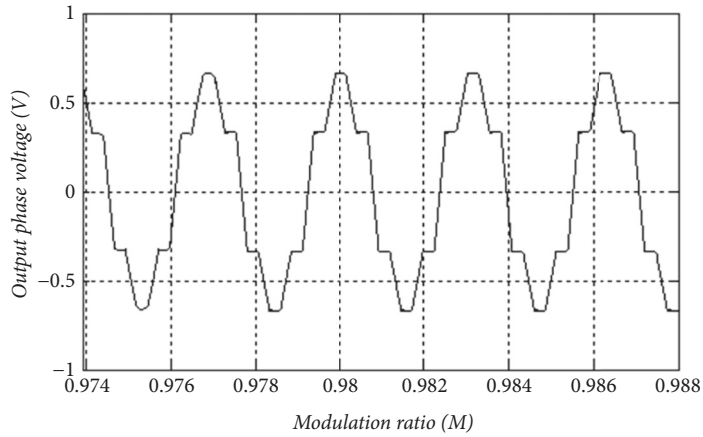

Figure 6: The relationship between fundamental amplitude of output phase voltage and m in mode II.

vector, the amplitude or phase of v_r must be adjusted so that the average value of output voltage for the entire period is equal to the reference voltage. The overmodulation coefficient of over modulation II is defined as

$$k_2 = \frac{m - m_2}{m_3 - m_2} \tag{15}$$

where m_3=0.988. In addition, the value of k_2 is set to 0 when voltage vector is located in overmodulation I, and the value of value of k_2 is set to 1 when voltage vector rotates along the regular dodecagon.

According to (8) and (9), the expression of v^* in sector 2 can be obtained by

$$\left|v^*\right| = \frac{2\left(\sqrt{3}+1\right)^2 V_{dc}}{24}\left(1 - k_2\right) + \frac{2\left(\sqrt{3}+1\right)^2 V_{dc}}{24\cos\left(\pi/6 - \varphi\right)}k_2 \tag{16}$$

In addition, when the reference voltage vector is located outside the regular dodecagon, an unreasonable situation that the dwell time of the zero vector is less than 0 will happen. So (3) is modified by

$$\begin{aligned} t_i &= \frac{t_i}{t_1 + t_2 + t_3 + t_4}, \quad i = 1, 2, 3, 4 \\ t_0 &= 0 \end{aligned} \tag{17}$$

Figure 6 shows the A phase voltage curve, in which V_{dc}=1V, and modulation ratio m increased from 0.974 to 0.988. As can be seen from the diagram, with the gradual increase of the modulation ratio m, the distortion of the output phase voltage is more and more obvious; when m is close to 0.988, the output voltage vector will rotate along the track of the regular dodecagon.

3.2.3. Overmodulation Region III (0.988 < m ≤ 1). The overmodulation coefficient of overmodulation III is defined as

$$k_3 = \frac{m - m_3}{1 - m_3} \tag{18}$$

where the value of k_3 is set to 0 when voltage vector is located in overmodulation II, and the value of k_3 is set to 1 when voltage vector rotates along the twelve-step wave.

Like overmodulation II region, to illustrate the process of adjusting the reference voltage vector, sector 2 shown in Figure 7 will be taken as an example, and V_{dod} and V_{twe} will be used to reconstruct the reference voltage vector v^*, i.e.,

$$v^* = V_{dod}\left(1 - k_3\right) + V_{twe}k_3 \tag{19}$$

Although the introduced V_{twe} vector makes the phase of reconstructed voltage vector different from the reference

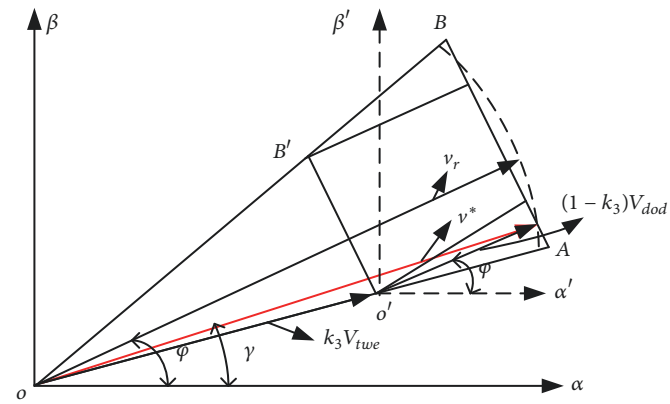

Figure 7: The principle diagram reference voltage vector in overmodulation section III.

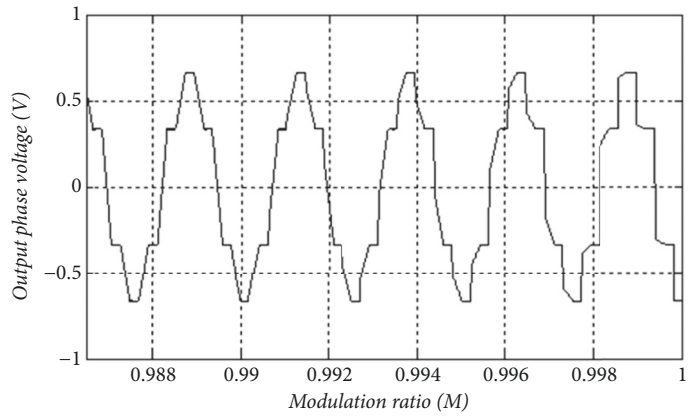

Figure 8: The relationship between fundamental amplitude of output phase voltage and m in mode III.

voltage vector, it increases the output amplitude of voltage vector. According to (9) and (10), the magnitude of the reconstructed voltage vector on the α-β axis can be obtained as

$$\begin{aligned}\left|v^*{}_\alpha\right| &= \frac{2\left(\sqrt{3}+1\right)^2\cos\varphi\cdot V_{dc}}{24\cos\left(\pi/6-\varphi\right)}\left(1-k_3\right)\\ &\quad+\frac{\sqrt{2}\left(\sqrt{3}+1\right)\cos\left(\pi/4\right)\cdot V_{dc}}{6}k_3\end{aligned} \tag{20}$$

$$\begin{aligned}\left|v^*{}_\beta\right| &= \frac{2\left(\sqrt{3}+1\right)^2\sin\varphi\cdot V_{dc}}{24\cos\left(\pi/6-\varphi\right)}\left(1-k_3\right)\\ &\quad+\frac{\sqrt{2}\left(\sqrt{3}+1\right)\sin\left(\pi/4\right)\cdot V_{dc}}{6}k_3\end{aligned} \tag{21}$$

The amplitude and phase of the reconstructed voltage vector can be obtained by

$$\begin{aligned}\left|v^*\right| &= \sqrt{\left|v^*{}_\alpha\right|^2+\left|v^*{}_\beta\right|^2}\\ \gamma &= \arctan\left(\frac{\left|v^*{}_\beta\right|}{\left|v^*{}_\alpha\right|}\right)\end{aligned} \tag{22}$$

Figure 8 shows the A phase voltage curve, in which V_{dc}=1V, and modulation ratio m increased from 0.987 to 1. As can be seen from the diagram, with the gradual increase of the modulation ratio m, the distortion of the output phase voltage is more and more obvious; when m is close to 1, the output voltage vector will rotate along the track of the regular dodecagon vertex.

4. Simulation Results Analysis

To verify the validity of the proposed SVPWM algorithm of six-phase VSI with wide modulation range, the simulation model is built in Matlab/Simulink environment. Figure 9 shows the phase voltage and phase voltage harmonic spectra in different modulation regions. The voltage is per unit value. When m=0.906, the harmonic voltages v_x and v_y are zero in x-y subspaces, and the phase voltage is sine wave, THD=0. As the modulation ratio increases, the THD of phase voltage gradually increases, and the low-order harmonic components are mainly from α-β subspace and x-y subspace.

Figure 10 shows the voltage vector of the different modulation ratios in the α-β and x-y subspaces. Among them, the left side of Figures 9(a), 9(b), and 9(c) is α-β subspace, and the right side is x-y subspace. It can be seen from

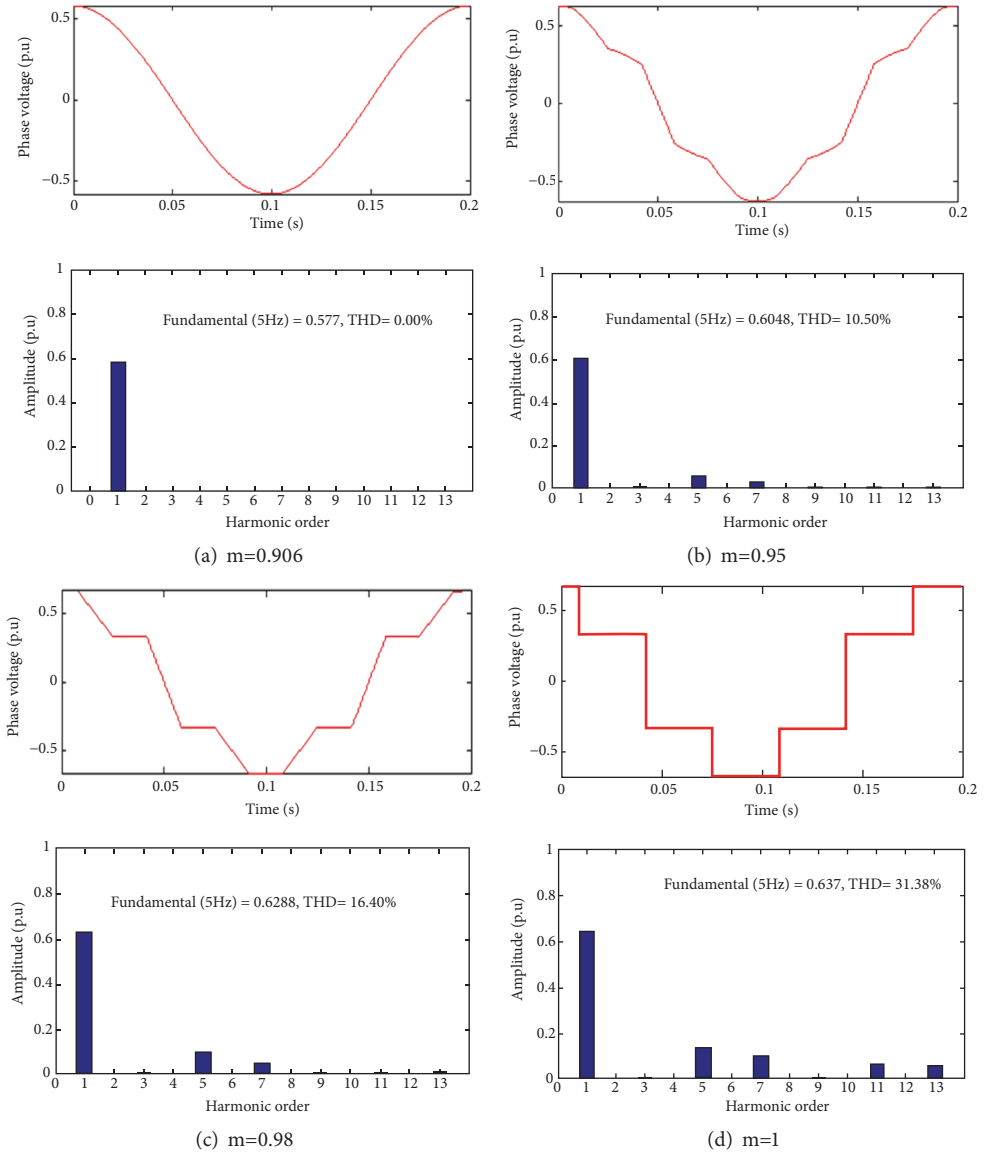

FIGURE 9: Phase voltage and phase voltage harmonic spectra in different modulation regions.

Figure 9, with the increase of the modulation ratio m, the fundamental amplitude of voltage vector on α-β subspace increases gradually, and the modulation ratio is m=0.988, the output voltage vector tracks along the regular dodecagon, and the output voltage vector trajectory rotates along the track of the regular dodecagon vertex with the modulation ratio of m=1, which verify the correctness of the above theory analysis.

In addition, although the harmonic component in the x-y subspace is gradually increasing, the utilization ratio of DC voltage is increased to a certain extent, and the distortion rate and harmonic content of phase voltage increase gradually, with the increase of modulation ratio. According to the above analysis, when the modulation ratio is higher than the linear modulation region (m>0.907), modulation strategy completely degenerates into two-vector SVPWM algorithm, the distortion rate of harmonic distribution is applicable to all the two-largest-vector synthesis, and only the harmonic amplitude is different.

Figure 11 shows the modulation curve of SVPWM method with different modulation ratio; it can be seen that when the modulation ratio is m=1, the modulation wave becomes a square wave signal.

To verify the validity of the proposed SVPWM algorithm achieves the smooth transitions from linear to overmodulation region, Figure 12 shows the curve of phase voltage, when the modulation ratio is m increased from 0.907 to 1. It can be seen that as the modulation ratio increases stepwise, the phase voltage waveform achieves a smooth transition from linear modulation region to overmodulation region.

In order to illustrate the superiority of the control algorithm proposed in this paper, Figure 13 shows the comparison with the traditional two-vector SVPWM algorithm and the simulation results. As can be seen from Figure 13, the THD

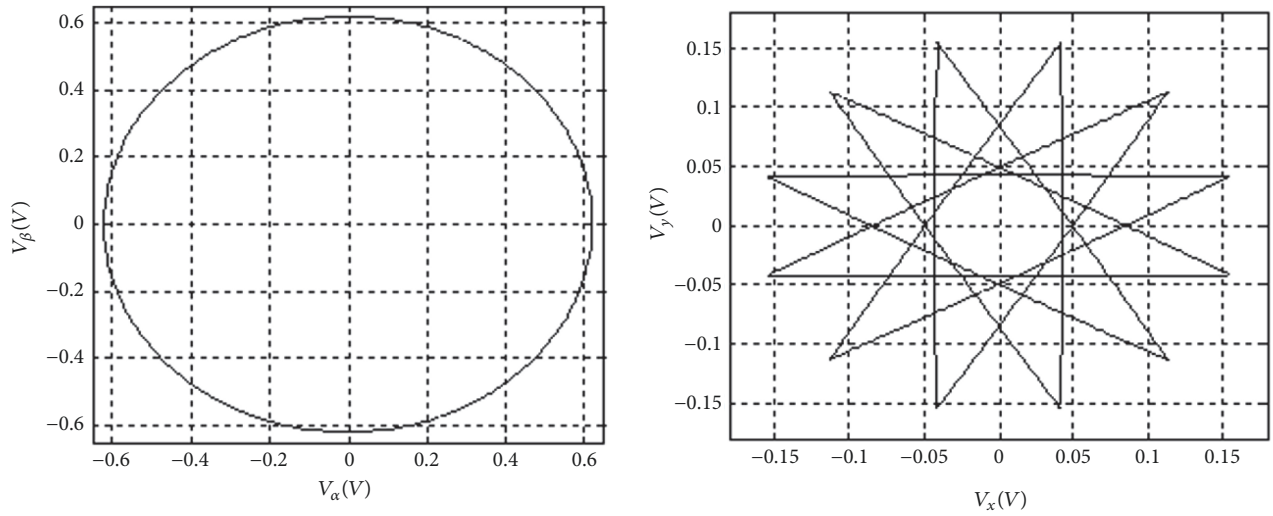

(a) Overmodulation region I (m=0.974)

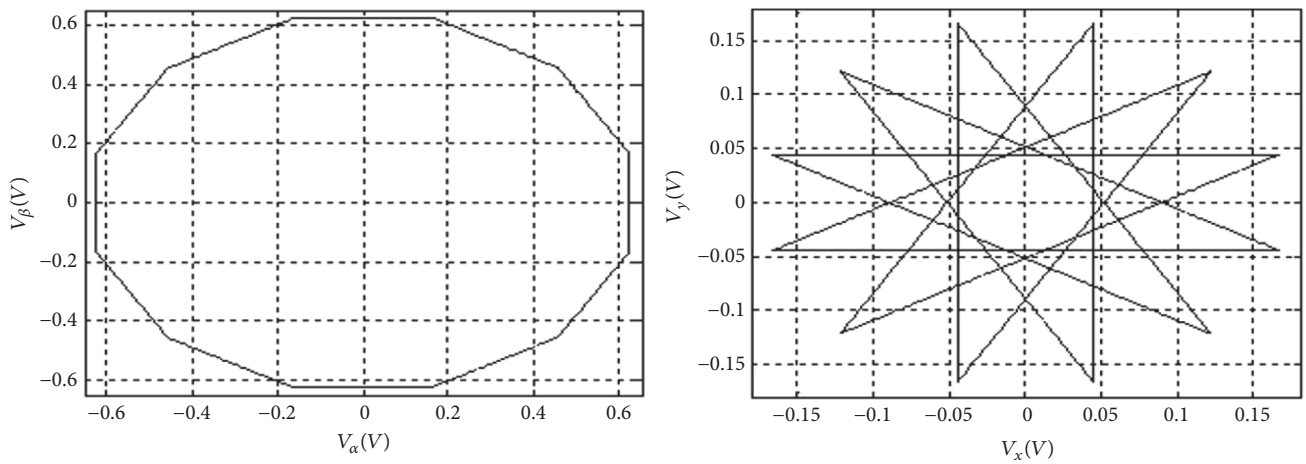

(b) Overmodulation region II(m=0.988)

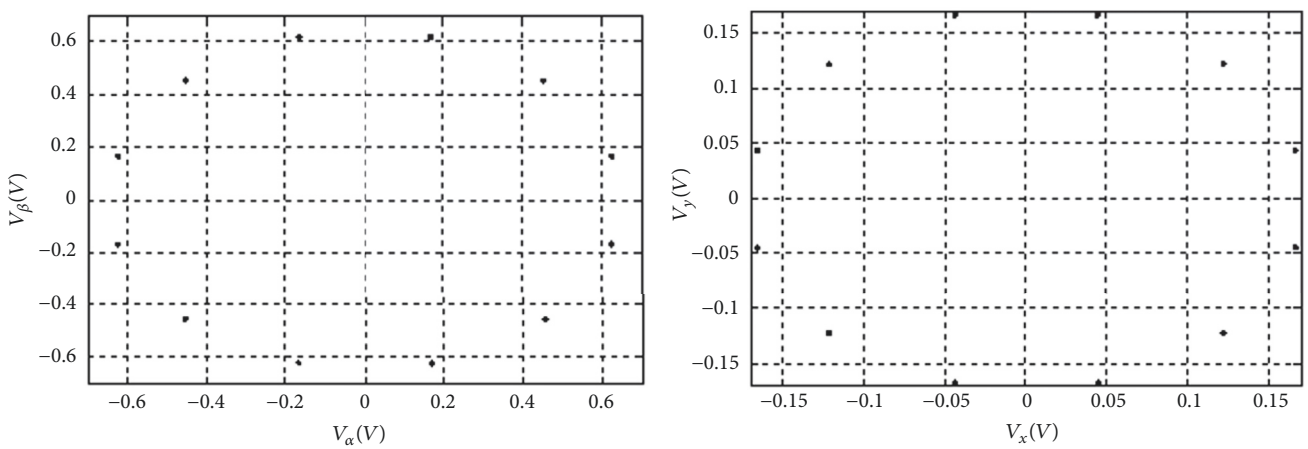

(c) Overmodulation region III(m=1)

Figure 10: The voltage vector of α-β and x-y subspaces in different modulation regions.

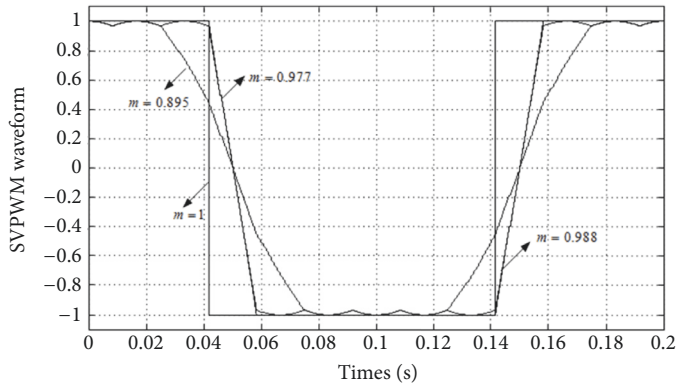

Figure 11: The modulated wave with different modulation ratio.

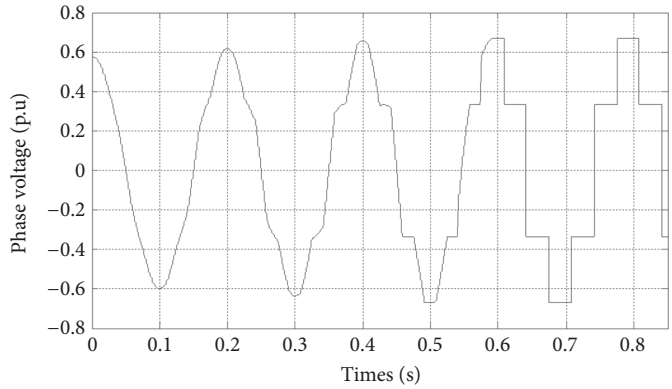

Figure 12: The modulated wave in different modulation regions.

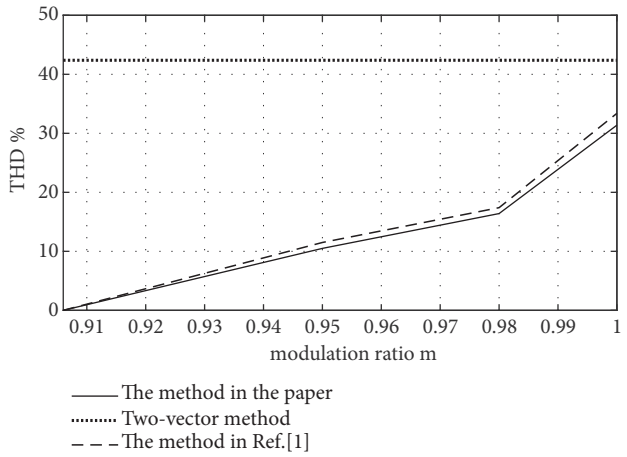

Figure 13: The comparison with the traditional two-vector SVPWM algorithm.

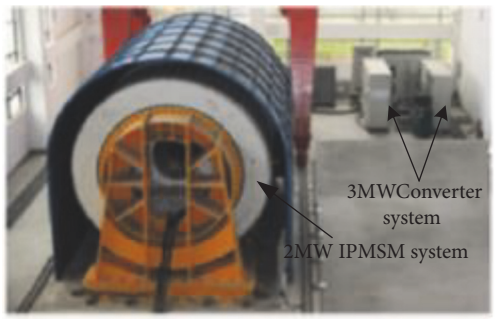

Figure 14: The overall experiment setup.

content of the proposed control strategy is relatively small. Thus, it is verified that the proposed algorithm has better control performance.

5. Experimental Results Analysis

To demonstrate the effectiveness of the proposed a novel SVPWM algorithm in full modulation region for six-phase voltage source inverter, the drive operation is examined at experiment platform shown in [19]. Figures 14 and 15 illustrate a 2MW IPMSM driving system and detailed experiment setup; a high-power back-to-back converter system is used to feed the IPMSM system and the parameters of IPMSM are present in Table 1. All three-phase currents and voltages are measured using magnetic current and voltage transducers.

The system control algorithms are developed in Matlab/Simulink, followed by implementation on an OPAL RT-Lab (Real-time Digital Simulator) controller board. In this paper, the method of changing the amplitude of a given signal is used to change the modulation ratio m value. The motor is controlled by V/F and the dead time is 10us. The phase voltage waveforms under different modulation degrees are observed

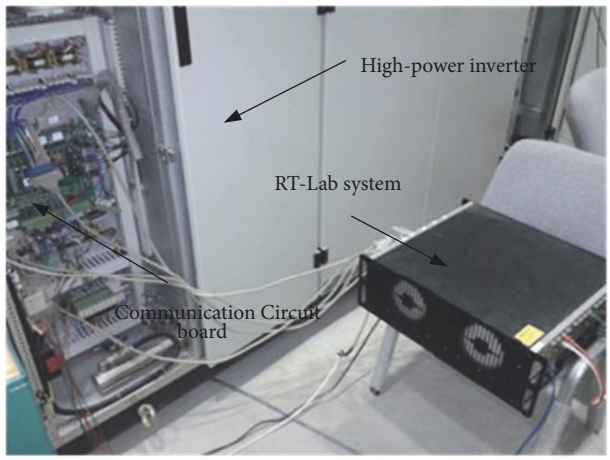

Figure 15: The detailed experiment setup.

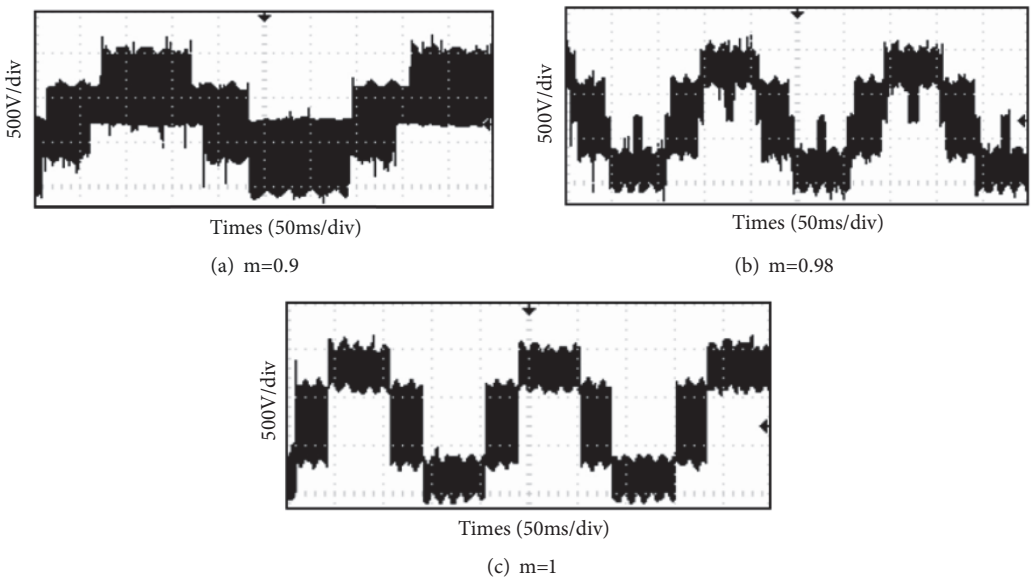

Figure 16: Phase A voltage experimental waveforms in different modulation index.

Table 1: Parameters of IPMSM prototype.

Rate power [kW]	2180
Rate speed [r/min]	17
Rate frequency [Hz]	8.5
Rotor inertia [kg·m^2]	16000
Rate phase to phase voltage [V(rms)]	690
Rate current [A]	1960
Number of pole pairs	30
Stator resistance per phase(R) [Ω]	0.0192
d-axis inductance (L_d) [mH]	4
q-axis inductance (L_q) [mH]	5
Permanent magnet flux (Ψ_f) [Wb]	10.228

by an oscilloscope as shown in Figure 16. It can be seen that with different modulation ratios along with the increasing modulation, the modulated wave in the PWM also gradually changes from a sine wave to a square wave signal. This is the same as the simulation result shown in Figure 9, and the phase voltage also transitions from the linear modulation region to the overmodulation region.

U_A and U_U phase voltage reconstruction waveforms are shown in Figure 17. It can be seen that the experimental waveform is consistent with the simulation waveform shown in Figure 10. Phase voltage U_U lags U_A 30 electrical angles. As the modulation index m increases, the voltage utilization rate increases gradually, and the phase voltage gradually transitions from a sine wave to a twelve-step wave.

6. Conclusion

To improve the utilization ratio of DC bus voltage and restrain the stator current harmonics and torque ripple, a novel

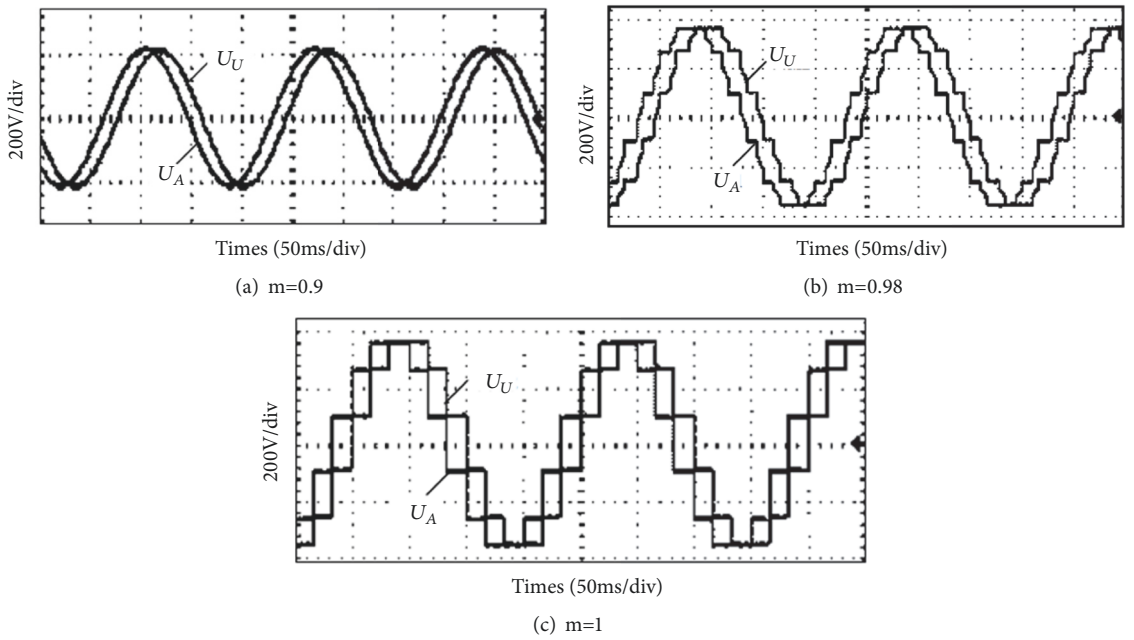

Figure 17: Phases A and U voltage experimental waveforms in different modulation index.

SVPWM modulation strategy based on vector space decoupling transform approach and vector weighting method is proposed in this paper. The overmodulation of the six-phase inverter is divided into 3 regions, such as overmodulation I, overmodulation II, and overmodulation III, and the dwell time of the SVPWM algorithm based on vector weighting method is deduced. Simulation and experimental analyses demonstrate the effectiveness and feasibility of the proposed strategy.

Data Availability

The data used to support the findings of this study are included within the article.

Conflicts of Interest

The authors declare no conflict of interest.

Authors' Contributions

All authors contributed to this article. Peng Wu and Lei Yuan designed the study and put forward the article's methods. They also participated in programming. Zhen Zuo collected a great deal of materials to form the article's structure as well as reviewing the manuscript. Junyu Wei carried out the simulations for the proposed methods and handled the experiments. All authors read and approved the final manuscript.

Acknowledgments

This work is supported by National Nature Science Foundation of China (under Grant 51507188) and Nature Science Foundation of HuNan province, China (under Grant 2019JJ50121).

References

[1] C. Zhou, G. Yang, and J. Su, "PWM strategy with minimum harmonic distortion for dual three-phase permanent-magnet synchronous motor drives operating in the overmodulation region," *IEEE Transactions on Power Electronics*, vol. 31, no. 2, pp. 1367–1380, 2016.

[2] X. Guo, M. He, and Y. Yang, "Over modulation strategy of power converters: A review," *IEEE Access*, 2018.

[3] E. E. M. Mohamed and M. A. Sayed, "Matrix converters and three-phase inverters fed linear induction motor drives—Performance compare," *Ain Shams Engineering Journal*, vol. 9, no. 3, pp. 329–340, 2018.

[4] Q. Luo, J. Zheng, Y. Sun, and L. Yang, "Optimal modeled six-phase space vector pulse width modulation method for stator voltage harmonic suppression," *Energies*, vol. 11, no. 10, article no. 2598, 2018.

[5] X. Tang, C. Lai, Z. Liu, and M. Zhang, "A SVPWM to eliminate common-mode voltage for multilevel inverters," *Energies*, vol. 10, no. 5, p. 715, 2017.

[6] M. Moranchel, F. Huerta, I. Sanz, E. Bueno, and F. J. Rodríguez, "A comparison of modulation techniques for modular multilevel converters," *Energies*, vol. 9, no. 12, p. 1091, 2016.

[7] L. Yuan, M.-L. Chen, J.-Q. Shen, and F. Xiao, "Current harmonics elimination control method for six-phase PM synchronous motor drives," *ISA Transactions*, vol. 59, pp. 443–449, 2015.

[8] L. Yuan, B. X. Hu, K. Y. We et al., "A novel current vector decomposition controller design for six-phase PMSM," *Journal of Central South University*, vol. 23, pp. 443–449, 2016.

[9] K. Hatua and V. T. Ranganathan, "Direct torque control schemes for split-phase induction machine," *IEEE Transactions on Industry Applications*, vol. 41, no. 5, pp. 1243–1254, 2005.

[10] Y. Zhao and T. A. Lipo, "Space vector PWM control of dual three-phase induction machine using vector space decomposition," *IEEE Transactions on Industry Applications*, vol. 31, no. 5, pp. 1100–1109, 1995.

[11] D. Dujic, M. Jones, and E. Levi, "Analysis of output current ripple rms in multiphase drives using space vector approach," *IEEE Transactions on Power Electronics*, vol. 24, no. 8, pp. 1926–1938, 2009.

[12] D. Dujic, M. Jones, and E. Levi, "Analysis of output current-ripple RMS in multiphase drives using polygon approach," *IEEE Transactions on Power Electronics*, vol. 25, no. 7, pp. 1838–1849, 2010.

[13] A. Iqbal and S. Moinuddin, "Comprehensive relationship between carrier-based PWM and space vector PWM in a five-phase VSI," *IEEE Transactions on Power Electronics*, vol. 24, no. 10, pp. 2379–2390, 2009.

[14] K. Marouani, L. Baghli, D. Hadiouche, A. Kheloui, and A. Rezzoug, "A new PWM strategy based on a 24-sector vector space decomposition for a six-phase VSI-Fed dual stator induction motor," *IEEE Transactions on Industrial Electronics*, vol. 55, no. 5, pp. 1910–1920, 2008.

[15] D. Hadiouche, L. Baghli, and A. Rezzoug, "Space-vector PWM techniques for dual three-phase ac machine: Analysis, performance evaluation, and DSP implementation," *IEEE Transactions on Industry Applications*, vol. 42, no. 4, pp. 1112–1122, 2006.

[16] S. Bolognani and M. Zigliotto, "Space vector Fourier analysis of SVM inverters in the overmodulation range," in *Proceedings of the International Conference on Power Electronics, Drives and Energy Systems for Industrial Growth*, pp. 319–324, New Delhi, India, 1996.

[17] D. Yazdani, S. Ali Khajehoddin, A. Bakhshai, and G. Joós, "Full utilization of the inverter in split-phase drives by means of a dual three-phase space vector classification algorithm," *IEEE Transactions on Industrial Electronics*, vol. 56, no. 1, pp. 120–129, 2009.

[18] G. Grandi, G. Serra, and A. Tani, "Space Vector Modulation of a Six-Phase VSI based on three-phase decomposition," in *Proceedings of the 2008 International Symposium on Power Electronics, Electrical Drives, Automation and Motion (SPEEDAM)*, pp. 674–679, Ischia, Italy, June 2008.

[19] L. Yuan, F. Xiao, J.-Q. Shen, M.-L. Chen, Q.-M. Shi, and L. Quan-feng, "Sensorless control of high-power interior permanentmagnet synchronous motor drives at very low speed," *IET Electric Power Applications*, vol. 7, no. 3, pp. 199–206, 2013.